Calcif Tissue Int (2015) 97:113–124
DOI 10.1007/s00223-015-9994-4

ORIGINAL RESEARCH

Deletion of Filamin A in Monocytes Protects Cortical and Trabecular Bone from Post-menopausal Changes in Bone Microarchitecture

S. Goldberg[1,2] · J. Glogauer[1] · M. D. Grynpas[2] · M. Glogauer[1]

Received: 3 February 2015 / Accepted: 1 April 2015 / Published online: 17 April 2015

Abstract The objective of the study was to determine the in vivo role of Filamin A (FLNA) in osteoclast generation and function, through the assessment of trabecular bone morphology, bone turnover, and the resulting changes in mechanical properties of the skeleton in mice with targeted deletion of FLNA in pre-osteoclasts. Using a conditional targeted knockdown of FLNA in osteoclasts, we assessed bone characteristics in vivo including micro-computed tomography (micro-ct), histomorphometric analyses, and bone mechanical properties. These parameters were assessed in female mice at 5 months of age, in an aging protocol (comparing 5-month-old and 11-month-old mice) and an osteoporosis protocol [ovariectomized (OVX) at 5 months of age and then sacrificed at 6 and 11 months of age]. In vivo bone densitometry, mechanical and histomorphometric analyses revealed a mild osteoporotic phenotype in the FLNA-null 5-month and aging groups. The WT and FLNA-KO bones did not appear to age differently. However, the volumetric bone mineral density decrease associated with OVX in WT is absent in FLNA-KO-OVX groups. The skeleton in the FLNA-KO-OVX group does not differ from the FLNA-KO group both in mechanical and structural properties as shown by mechanical testing of femora and vertebrae and histomorphometry of vertebrae. Additionally, FLNA-KO femora are tougher and more ductile than WT femora. The result of this study indicates that while FLNA-KO bones are weaker than WT bones, they do not age differently and are protected from estrogen-mediated post-menopausal osteoporosis.

Keywords FLNA · Bone turnover · Osteoporosis · Aging

✉ S. Goldberg
Michael.glogauer@utoronto.ca

[1] Matrix Dynamics Group- Faculty of Dentistry, Fitzgerald Building 150 College Street, Toronto, ON M5S3E2, Canada

[2] Lunenfeld-Tanenbaum Research Institute, Mount Sinai Hospital, 600 University Ave, Toronto, ON M5G1X5, Canada

Introduction

Bone is a dynamic tissue that is continually remodeled to provide maximal strength with minimal mass as determined by the physiological needs of vertebrate organisms [1]. Bone formation and resorption are metabolic processes accomplished through the precise coordination of osteoblast and osteoclast activity. Osteoblasts of mesenchymal origin deposit the calcified bone matrix, while osteoclasts of haematopoietic origin resorb bone [2]. Osteoclasts are large multinucleated cells, the only cells capable of resorbing bone. Osteoclasts are highly polarized cells requiring dynamic cytoskeletal reorganization in order to adhere, migrate, and resorb bone mineral and matrix [3, 4].

Diseases such as osteoporosis, caused by excessive bone turnover, can result in fractures that can cause morbidity, shortened lifespan, and weakened skeletal structure [5, 6]. Osteoporosis is characterized by low bone mass and deterioration of bone architecture [7]. One of the major consequences of osteoporosis is disturbed bone architecture resulting in fractures, which places a significant economic burden on the healthcare system [8]. Up-regulation of bone turnover through mechanisms not clearly defined is a direct result of estrogen depletion leading to post-menopausal osteoporosis [9]. Ovariectomy (OVX) is a valuable tool used in numerous animal models to mimic estrogen depletion in post-menopausal women. Estrogen deficiency

leads to stimulation of bone resorption and formation through prolonging and shortening the lifespan of osteoclasts and osteoblasts, respectively. As a consequence, a high turnover state develops which leads to bone loss and perforation of trabecular plates [10, 11].

Following stimulation by cytokines RANKL and M-CSF, osteoclasts are formed [osteoclastogenesis (OCG)] through mononuclear monocyte fusion derived from hematopoietic progenitors in the bone marrow. In vivo, OCG is supported by cell-to-cell contact between expressed RANKL on the surface of osteoblasts and RANKL receptor on the surface of osteoclast precursor cells [2]. Migration is a crucial cellular event in osteoclast formation and function as it brings cells in close proximity prior to fusion to enable the formation of mature multinucleated osteoclasts [2, 12]. Cellular migration and membrane fusion require dynamic actin cytoskeleton reorganization achieved through Rho family small GTPase (Rac1, Cdc42, and RhoA) activity [12–14]. Recent literature postulates that the flexible hinge region of actin-binding protein Filamin A (FLNA) localizes Rho GTPase signaling intermediates within close proximity to each other to facilitate efficient actin cytoskeletal remodeling.

FLNA is a ubiquitous actin-binding protein that cross-links cortical F-actin into three-dimensional orthogonal networks at the leading edge of cells in X-, T-, or Y-shaped junctions. FLNA is the most abundant and widely expressed isoform among Filamins A, B, and C, sharing 70 % sequence homology [15–17]. FLNA is required for podosome and sealing zone formation in osteoclasts. It binds the integrin beta subunit cytoplasmic domain to allow the spatial and temporal organization of different integrin-linked F-actin meshworks [18]. FLNA is critical for normal cortical neuron migration from their native neural crest location to the cerebral cortex during brain development. A null mutation in the FLNA gene results in defective migration of neurons in the lateral ventricle leading to periventricular heterotopia (PVNH). The FLNA-deficient M2 cell line, derived from human malignant melanoma, also exhibits defective migratory ability that is restored upon FLNA transgene rescue [19].

Deficiencies in OCG in FLNA-null monocytes were observed in recent in vitro studies and preliminary in vivo studies. Under normal in vitro plating densities, FLNA-null osteoclasts were smaller, less numerous, and contained less nuclei per osteoclast. Quantification of osteoclasts in vivo in the distal femoral head of male mice revealed similar results, illustrating the in vivo physiological relevance of FLNA in OCG. Further preliminary findings of reduced OCG in vivo in male mice suggest a possible skeletal phenotype of osteopetrosis, with or without concomitant defects in bone remodeling [19]. The aforementioned results raised the question of how deletion of FLNA would impact female mice in vivo and how the deletion of FLNA and lack of estrogen would fare on these mice. Our hypothesis was that deletion of FLNA in a transgenic mouse model would result in an osteopetrotic phenotype where FLNA-KO mice will have fewer active osteoclasts and/or reduced bone remodeling. Our model aims to assess the in vivo impact of the loss of FLNA on the bony skeleton and its impact on aging and OVX transgenic mice. This was achieved using 5-, 6-, and 11-month-old FLNA-WT and FLNA-KO mice ($n = 15$ per group). The 5-month group was used to assess whether there was a phenotype upon loss of FLNA. The 11-month group was compared to the 5-month group to study the physiological effects of aging and to determine whether WT mice age differently from FLNA-KO mice. Mice were ovariectomized (OVX) at 5 months of age and then sacrificed at 6 and 11 months of age to establish an osteoporosis model for loss of FLNA. In vivo micro-ct, mechanical testing, and histomorphometry were used to characterize the role of FLNA in osteoclast generation, trabecular bone morphology, bone turnover, and the consequences of the lack of FLNA in aging mice and upon estrogen depletion.

Materials and Methods

Animals

All procedures described were performed in accordance with the Guide for the Humane Use and Care of Laboratory Animals and were approved by the University of Toronto Animal Care Committee. SV129-black 6 mice containing the conditional knockout of the X-linked FLNA gene (FLNA-null) were generated as described previously [20, 21]. Since a global knockout resulted in lethality, a conditional knockout strategy was used with loxP sites inserted into introns 2 and 7 of the mouse FLNA gene (FLNAc/c or male FLNAc/y mice). Deletion of the FLNA gene in granulocytes (neutrophils and monocytes) was accomplished by breeding these mice with mice expressing cre-recombinase under control of the granulocyte-specific lysozyme M promoter that is active during early embryogenesis [22]. Cre-mediated recombination deletes exons 3–7, producing a non-sense mutation with early FLNA truncation at amino acid 121. To confirm deletion of the FLNA gene, tail snips were used to prepare DNA for PCR analysis as described previously [20]. Littermates with unsuccessful cre-mediated recombination were used as wild-type control (WT) [22]. For the purposes of this study, ten groups of mice containing WT and FLNA-KO mice were used. Each group comprised 15 mice for a total of 150 mice to establish statistical significance and guard against losses.

In order to investigate bone characteristics in mice missing this important protein for bone resorption, 5-month-old WT and FLNA-KO female mice were compared with each other and for the aging model, to 11-month-old WT and FLNA-KO mice ($n = 15$ per group). Mice were ovariectomized (OVX) at 5 months of age and then sacrificed at 6 and 11 months to establish osteoporosis models for loss of FLNA. The 11-month group was utilized to study the natural physiological aging model of osteoporosis as well as the extreme case of osteoporosis, which is induced by OVX. No significant differences were reported at the tissue level for bone resorption and formation in vivo. The 6-month group was introduced to ensure that the effects due to OVX were taking place at the tissue level, which takes place 4–6 weeks post-surgery. Femur bones and 6th lumbar vertebrae were placed in saline-soaked gauze and frozen. Specimens were thawed overnight prior to use for micro-ct and mechanical testing.

Calcein green is a bone formation marker that is preferentially taken up at the site of active mineralization of bone [23]. Two and ten days before euthanasia 5-, 6-, and 11-month-old OVX mice were injected in their peritoneal cavities with calcein green (30 mg/kg) for bone dynamic histomorphometric analysis. Animals were sacrificed by CO2 asphyxiation, following animal care protocol established by University of Toronto Animal Care Committee.

Bone Densitometry and Structural (BMD) Analyses

Micro-computed tomography (micro-ct) is a tool used to create high-resolution ($\sim$6 microns) three-dimensional images of the bone and for the calculation of volumetric BMD (vBMD) (g/cm^3) as well as to evaluate changes in trabecular bone microarchitecture. Micro-ct was performed on right femora and sixth lumbar vertebrae from 5- to 11-month-old mice. Femora and sixth lumbar vertebrae, trimmed to leave only the vertebral body, were mounted in microtubes and scanned using SkyScan 1172 micro-ct scanner (Bruker). Femora and vertebrae were scanned at 11.6 and 6.1 μm resolutions, respectively. All images were obtained at an x-ray voltage of 50 kV and current of 800 A with a 0.25 mm aluminum filter to ensure a uniform beam. All scans were reconstructed and calibrated with the use of two hydroxyapatite standards that were provided by the manufacturer. Reconstructed images obtained from scanning were analyzed using the Skyscan CT-Analyzer software (Version 1.6.1). Femoral geometry and vBMD were assessed from the analysis of a region of interest created 0.25 mm above and below the midpoint. Femoral midpoints were measured by the use of digital calipers and serve as the points of fracture for three-point bending tests. The density parameter considered was volumetric bone mineral density (vBMD), and the structural parameters analyzed were bone area (B.Ar (mm^2)), cross-sectional thickness [Cs.Th (mm)], and anterior–posterior diameter (A–P (mm)). Vertebral trabecular architecture and vBMD were assessed by creating a region of interest along the length of the vertebrae but with exclusion of vertebral growth plates. Structural parameters analyzed for vertebrae included percentage of bone volume [BV/TV (%)], trabecular thickness [Tb.Th (mm)], trabecular number (Tb.N), and trabecular separation [Tb.Sp (mm)].

Mechanical Testing

Right femora from 5- to 11-month-old mice were tested in three-point bending to evaluate the mechanical properties of cortical bones. Sixth lumbar vertebrae were tested in compression to evaluate the properties of trabecular bones.

Three-point bending and vertebral compression were performed using an Instron 4465 materials testing machine (Instron Canada Inc.). A pre-load of less than 1 N was applied to establish each sample's contact with the upper device. Further load was applied by a 100 N cell load at a speed of 1 mm/min, and load versus time data were collected every 0.1 s by LabView data acquisition software (National Instruments Corp.; Austin, TX) until sample failure. Digital calipers were used to calculate femoral midpoints. Femora were positioned between two supports, 6 mm apart, with the posterior side facing downwards.

Vertebral body height and area were measured for data normalization. All vertebrae were carefully removed of any adherent soft tissue that may remain from the intervertebral disks allowing for the proximal and distal ends of the vertebra to be as flat as possible for testing purposes. A fine layer of cyanoacrylate-based adhesive was then applied to a metal plate to securely adhere the distal vertebrae so that its length is perpendicular to the plate.

Displacement was automatically calculated based on speed and time, and a load–displacement graph was generated to evaluate bones' structural mechanical properties such as ultimate load (N), energy to failure (mJ), and stiffness (N/mm). Afterward, data were normalized to the bone cross section and height for femora and vertebrae, respectively. A stress–strain graph was generated to evaluate the material properties of bones such as ultimate stress (GPa), failure strain (%), toughness (Gpa), and modulus (GPa).

Static and Dynamic Histomorphometric Analysis

Fifth lumbar vertebrae from 5-, 6-, and 11-month-old WT and FLNA-KO mice were isolated and fixed in 70 % ethanol. Samples were dehydrated in ascending concentrations of acetone followed by ascending ratios of

unpolymerized spur resin and acetone. Afterward, bones were embedded in blocks of spur resin and left to polymerize in a 60 C oven for 48 h. Using a semiautomatic microtome (Leica RM 2265), three 5-micron-thick coronal sections were cut from each sample and placed on gelatinized slides for Goldner's trichrome staining [22]. One 7-micron-thick coronal section was cut, placed on gelatinized slides. and left unstained for dynamic histomorphometric analysis. Trabecular bone was analyzed using a 25× objective lens connected to a video camera (Retiga 1300). Serial fields using the Leitz Bioquant morphometry system (Bioquant Nova Prime version 6.50.10) were analyzed from each sample to determine the following static histomorphometric formation parameters including osteoid volume [OV (mm^3)], osteoid surface [OS (mm)], and osteoid thickness [O.Th. (mm)] (Image 1a).

Dynamic histomorphometry was performed using fluorescence microscopy to measure the bone labels generated by calcein-green-injected mice prior to euthanasia. All mice in this study were given two single intraperitoneal injections of calcein green (0.6 % calcein green; 30 mg/kg rodent) at 10 and 2 days before animal sacrifice. The single and double calcein-green labels were measured on trabecular bone to calculate mineralizing surface [MS (mm)], percentage mineralizing surface (%.MS), mineral apposition rate [MAR (μm/day)], and bone formation rate [BFR (μm/day)]. All parameters are in accordance with the histomorphometric nomenclature and definition of the American Society of Bone Mineral Research (ASBMR) (Image 1b) [23].

TRAP Staining Analysis

Fourth lumbar vertebrae were isolated from 5-, 6-, and 11-month-old WT and FLNA-KO mice and fixed in 10 % formalin. Samples were decalcified using ethylenediaminetetraacetic acid (EDTA, 0.5 M, pH 7.4) at 4C, with daily solution changes for 8 weeks. Complete decalcification was confirmed by faxitron imaging. Decalcified samples were then processed (series of formalin, 70 % ethanol, 90 % ethanol, 100 % ethanol, 100 % xylene, and paraffin) and embedded in bone-specific paraffin. 5-micron-thick coronal sections were cut serially using a Leica Reichert Jung 2030 microtome (Leica Microsystems Canada Inc., Richmond Hill, Ontario) and mounted on Superfrost Plus (high section adhesion) glass slides. The Acid Phosphatase Leukocyte kit and protocol (Procedure No. 386, Sigma-Aldrich Canada Ltd., Oakville, Ontario) were used to prepare and perform TRAP staining. Slides were incubated in the TRAP stain at 37C for 1 h with periodic shaking. Following incubation, slides were washed and counterstained with Acid Hematoxylin. Slides were cover-slipped using a water-soluble mounting media (Aqua Perm) and were allowed to dry overnight in a 37C oven prior to analysis.

Three 5-micron-thick coronal sections were cut serially from each sample and placed on glass slides for Tartrate-Resistant Acid Phosphatase (TRAP) staining. Osteoclasts selectively express and stain positive for the TRAP enzyme. The Leitz Bioquant morphometry system was used to quantify the number of osteoclasts (Oc.N.), osteoclasts surface [Oc.S. (mm)], percent osteoclasts surface (%.Oc.S.), number of osteoclasts per bone surface (N.Oc/BS), and number of osteoclasts per osteoclasts surface (N.Oc/Oc.S) (Image 1c).

Statistical Analysis

For all analyses, SPSS (version 22.0) was used. One-way Analysis of Variance (ANOVA, general linear model) was used to compare the measured parameters between groups. A p value of <0.1 was required for a trend between 5-month groups. A p value of <0.05 was required to consider a significant difference in all other groups. All results are presented as mean ± standard deviation (SD) in graphs and means in tables.

Results

Phenotype of 5-Month-Old FLNA-KO Mice at Macro, Cellular and Tissue Levels

Micro-ct was performed on 5-month-old WT and FLNA-KO right femora and 6th lumbar vertebrae to assess cortical and trabecular vBMD and geometry, respectively. Mean vBMD and cross-sectional thickness were significantly reduced in 5-month FLNA-KO cortices compared to WT cortices (Fig. 1a, b, respectively). vBMD and trabecular number (Tb.N) were significantly reduced, while trabecular separation (Tb.Sp) was significantly increased ($p < 0.1$) in FLNA-KO compared to WT trabeculae (Fig. 1c, d, e). Three-point bending data revealed that ultimate load and stiffness were significantly decreased in 5-month FLNA-KO femora compared to WT femora (Fig. 2a, b). Upon normalization of the load–displacement data, only ultimate stress was reduced in FLNA-KO femora compared to WT femora ($p < 0.1$). The data suggest that FLNA-KO femora are weaker than WT femora. Vertebral compression data show that post-yield displacement and plastic energy are increased in FLNA-KO vertebrae compared to WT vertebrae suggesting that WT vertebrae are slightly more brittle than FLNA-KO vertebrae ($p < 0.1$). No significant differences were observed at the cellular and tissue levels for bone resorption and bone formation rates between WT and FLNA-KO vertebrae.

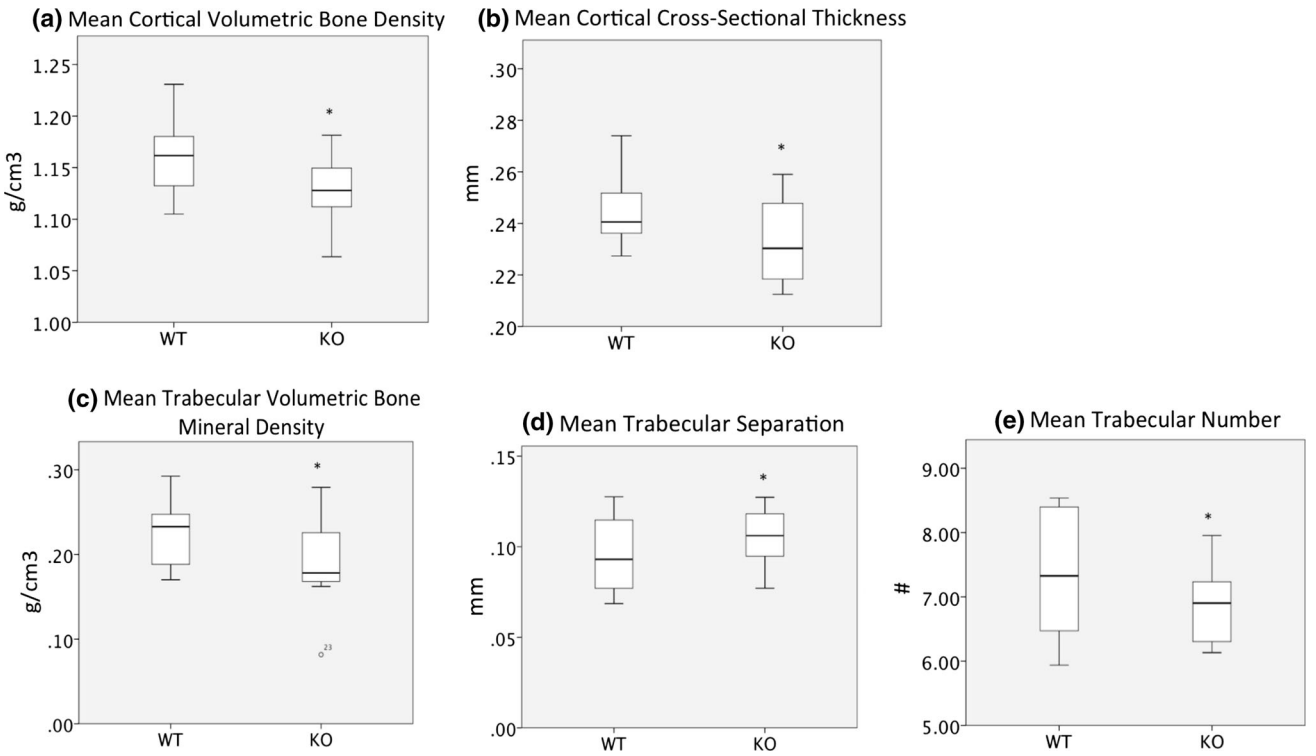

Fig. 1 5-month-old FLNA-KO bones have reduced bone mineral density and geometric properties compared to 5-month-old WT bones. Mean volumetric bone mineral density and cross-sectional thickness are significantly decreased in FLNA-KO femora (Fig. 1**a**, **b**). Mean volumetric bone mineral density and trabecular number are significantly decreased, while trabecular separation is significantly increased in FLNA-KO vertebrae (Fig. 1**c**, **d**, **e**). *Stars* represent data that are significantly decreased ($p < 0.1$)

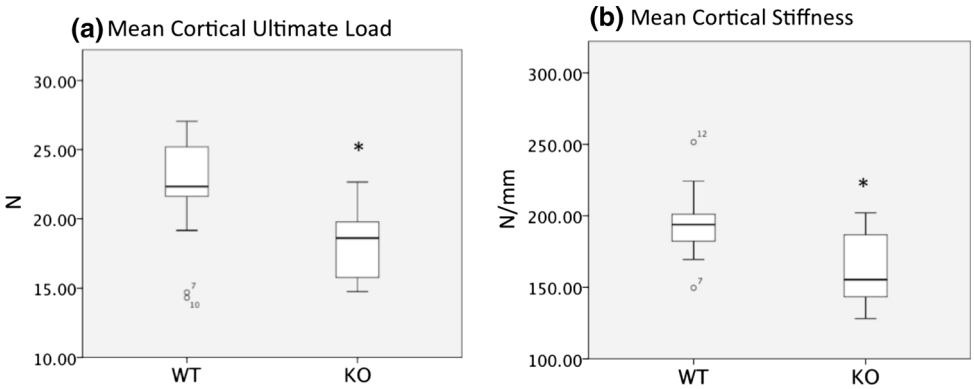

Fig. 2 5-month FLNA-KO femora have reduced mechanical properties compared to 5-month WT femora. Mean ultimate load and stiffness are significantly decreased in FLNA-KO femora (Fig. 2**a**, **b**). *Stars* represent data that are significantly decreased ($p < 0.1$)

Phenotype of FLNA-WT and FLNA-KO Aging Mice (5 months→11 months) at Macro, Cellular, and Tissue Levels

Micro-ct was performed on 11-month-old WT and FLNA-KO femora and vertebrae to assess cortical and vertebral vBMD and geometry, respectively. Results were compared to the 5-month groups to determine whether skeletal aging differs between WT and FLNA-KO mice. Mean bone area of femora was significantly increased in the WT aging group (5 months vs. 11 months) (Table 1). FLNA-KO femora showed significant increases in both vBMD and bone area at 11 months (Table 1). Trabecular separation was significantly increased, while trabecular number was significantly decreased in both WT and FLNA-KO vertebrae in 11-month groups (Table 2). Vertebral vBMD was significantly increased in the 11-month FLNA-KO aging group (Table 2). Three-point bending data of femora revealed that only normalized parameters including ultimate stress and modulus were significantly decreased in both WT and FLNA-KO 11-month groups (Table 3). No significant differences were reported between 5- and

Table 1 Micro-CT of aging femora

Parameter	5-month WT	11-month WT	5-month KO	11-month KO	*p* value WT	*p* value KO
vBMD (g/cm^3)	1.16 ± 0.035	1.18 ± 0.050	1.13 ± 0.036	1.17 ± 0.044	0.37	0.01*
Bone area (mm^2)	1.03 ± 0.1	1.18 ± 0.119	0.97 ± 0.085	1.1 ± 0.108	0.002*	0.001*
Cross-sectional-thickness (mm)	0.24 ± 0.013	0.25 ± 0.019	0.23 ± 0.015	0.24 ± 0.018	0.6	0.07

Mean bone area was significantly increased in WT 11-month-old femora. The FLNA-KO group showed significant increases in both vBMD and bone area at 11 months. Table represents mean ± SD

* Significant difference at $p < 0.05$

Table 2 Micro-CT of aging vertebrae

Parameters	5-month WT	11-month WT	5-month KO	11-month KO	*p* value WT	*p* value KO
vBMD (g/cm^3)	0.23 ± 0.033	0.21 ± 0.081	0.19 ± 0.068	0.15 ± 0.068	0.59	0.07
BV/TV (%)	32.46 ± 4.617	27.94 ± 11.54	28.55 ± 9.419	22.69 ± 7.211	0.18	0.01*
Tb.Th (mm)	0.043 ± 0.004	0.04 ± 0.011	0.04 ± 0.012	0.04 ± 0.012	0.77	0.92
Tb.Sp (mm)	0.09 ± 0.015	0.12 ± 0.056	0.10 ± 0.0312	0.14 ± 0.043	0.02*	0.0001*
Tb.N (#)	7.36 ± 0.756	6.02 ± 1.276	6.85 ± 1.915	5.45 ± 1.649	0.002*	0.0001*

Trabecular separation was significantly increased, while trabecular number was significantly decreased in both WT and FLNA-KO 11-month-old vertebrae. vBMD was significantly increased in 11-month FLNA-KO vertebrae. Tables represent mean ± SD

* Significant difference at $p < 0.05$

Table 3 Three-point bending of aging femora

Parameters	5-month WT	11-month WT	5-month KO	11-month KO	*p* value WT	*p* value KO
Ultimate load	22.22 ± 3.923	20.76 ± 3.871	18.14 ± 2.62	18.67 ± 5.28	0.31	0.75
Fail displace	0.27 ± 0.115	0.24 ± 0.105	0.29 ± 0.09	0.33 ± 0.13	0.75	0.38
Energy-to-fail	3.93 ± 2.034	3.13 ± 1.350	3.61 ± 1.56	4.18 ± 2.09	0.44	0.41
Stiffness	194.3 ± 24.24	198.0 ± 43.04	161.0 ± 25.4	165.15 ± 36.59	0.95	0.72
Ultimate stress	131.4 ± 21.37	98.51 ± 24.35	119.1 ± 13.78	93.68 ± 19.99	0.001*	0.0001*
Fail strain	5.79 ± 2.548	5.35 ± 2.431	6 ± 1.480	7.48 ± 3.03	0.93	0.12
Modulus	5504.8 ± 984.1	4068.3 ± 1352.0	5168.4 ± 985.6	3713.5 ± 849.4	0.007*	0.0001*
Toughness	4.92	3.35	4.84	4.71	0.15	0.85

Three-point bending data of femora revealed that only normalized parameters including ultimate stress and modulus were significantly decreased in both WT and FLNA-KO 11-month groups. All results are reported as means in tables. A *p* value of < 0.05 was required for significance. Tables represent mean ± SD

* Significant difference at $p < 0.05$

11-month groups in both the WT and FLNA-KO categories for vertebral compression, TRAP, static and dynamic histomorphometry. Taken together, the data reveal that there are slight skeletal aging changes in each of the WT and FLNA-KO groups but that FLNA deletion does not impact on age-related skeletal changes.

Phenotype of FLNA-WT and FLNA-KO-OVX Mice at Macro, Cellular, and Tissue Levels

Post-OVX, 11-month WT-OVX femora show expected significant decreases in vBMD compared to the FLNA-WT sham group. No difference was reported between FLNA-KO sham and FLNA-KO-OVX femora (Fig. 4a). Femoral geometry reveals that there is a significant effect due to OVX in femora of the WT group for B.Ar and Cs.Th; however, this effect is not evident in FLNA-KO groups (Fig. 3b). Upon estrogen depletion, vBMD was significantly reduced in WT-OVX vertebrae compared to WT vertebrae (Fig. 3c). FLNA-KO-OVX vertebrae did not differ significantly from the WT-OVX vertebrae as well as FLNA-KO sham vertebrae (Fig. 3c). BV/TV was significantly decreased and Tb.Sp. was significantly increased in WT-OVX vertebrae compared to WT sham vertebrae (Fig. 3d, e). These parameters did not differ significantly between the FLNA-KO-OVX and the FLNA-KO sham vertebrae.

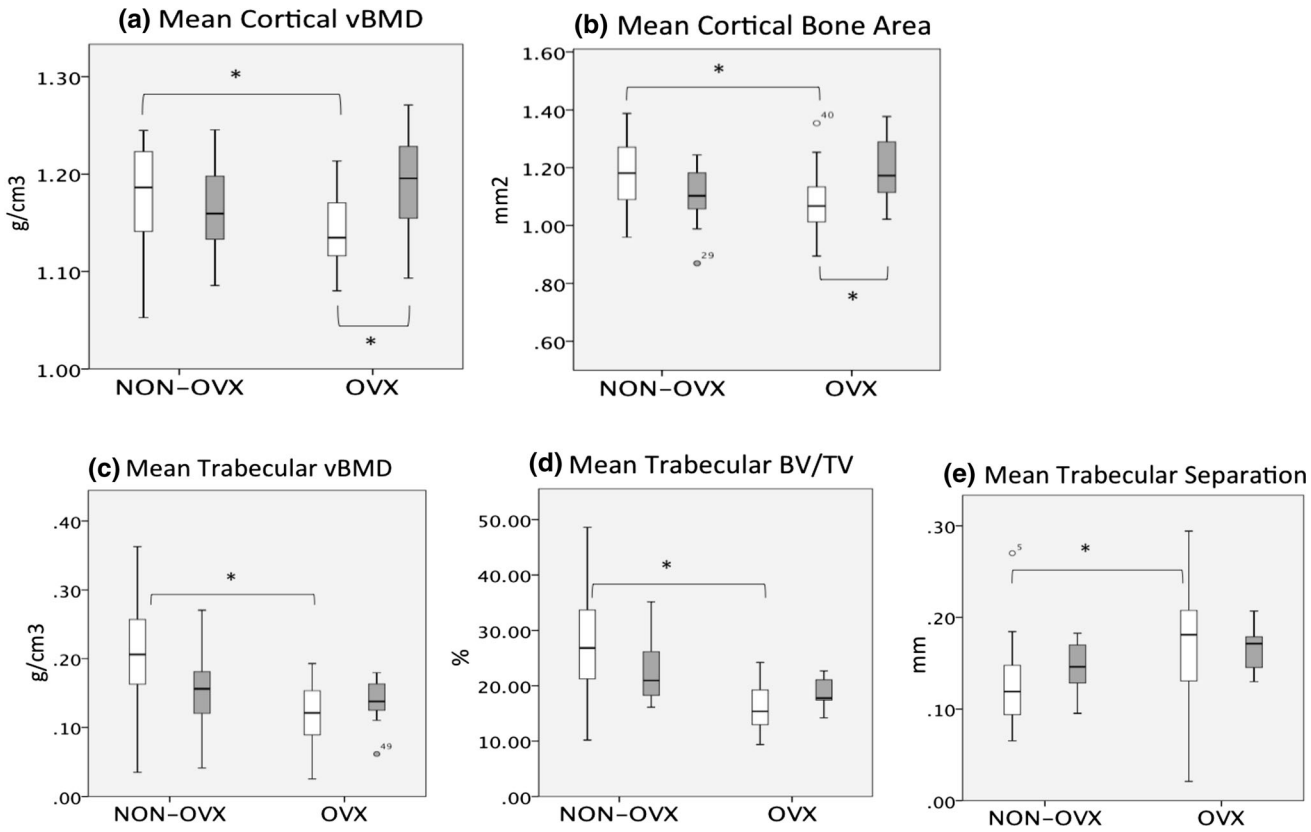

Fig. 3 FLNA-KO femora and vertebrae are protected from post-menopausal changes in material and geometric properties of bone. WT-OVX femora show expected significant decreases in vBMD in the 11-month group. No significance was reported between FLNA-KO sham and FLNA-KO-OVX femora. Femoral geometry reveals that there is a significant effect due to OVX in the WT group for B.Ar of femora; however, FLNA-KO groups remain unchanged from one another (Fig. 3**a**, **b**). vBMD was significantly reduced in 11-month-old WT-OVX vertebrae. FLNA-KO-OVX vertebrae did not differ significantly from the WT-OVX group as well as the FLNA-KO sham group (Fig. 3**c**). The same phenomena were observed for vertebral geometry including BV/TV and Tb.S (Figs. 3**d**, **e**, respectively). *Stars* represent data that are significantly decreased ($p < 0.05$)

With OVX, ultimate load, fail displacement, energy to fail, and stiffness are significantly decreased in 11-month WT-OVX femora (Fig. 4a). Following normalization of the load–displacement data, ultimate stress, fail strain, and modulus are significantly decreased in WT-OVX femora compared to the WT non-OVX group (Fig. 4). The significant reduction in the structural and material properties of femora due to OVX in the WT groups is not observed among FLNA-KO groups. Structurally, FLNA-KO and FLNA-KO-OVX femora require more energy to fracture compared to WT and WT-OVX femora (Fig. 4). When structural properties were normalized to cross-sectional area of femora, the failure strain was significantly increased in FLNA-KO and FLNA-KO-OVX mice compared to WT and WT-OVX mice (Fig. 4). These data would suggest that FLNA-KO and FLNA-KO-OVX femora are more ductile than WT and WT-OVX femora. The more the energy dissipating (or toughening) mechanisms exist, the more difficult it is to break a material.

As mentioned above, stiffness as well as Young's modulus is significantly decreased in the WT-OVX femora compared to the WT femora (Fig. 4). FLNA-KO femora and FLNA-KO-OVX femora remain unchanged from one another and are significantly different from the WT-OVX group. Together, these data suggest that FLNA-KO cortices are protected from estrogen-mediated post-menopausal submission to fracture and are more ductile than WT.

Vertebral compression data show expected significant decreases in the WT-OVX group for ultimate load and stiffness. FLNA-KO vertebrae are not significantly different from FLNA-KO-OVX vertebrae (Fig. 5a, b, respectively). It should be mentioned that for the aforementioned parameters, the FLNA-KO non-OVX group is still lower than the WT non-OVX group but is only significant at $p < 0.1$ which was the contingency for significance in the 5-month group.

TRAP staining revealed no significant differences in osteoclast parameters between WT, FLNA-KO, WT-OVX,

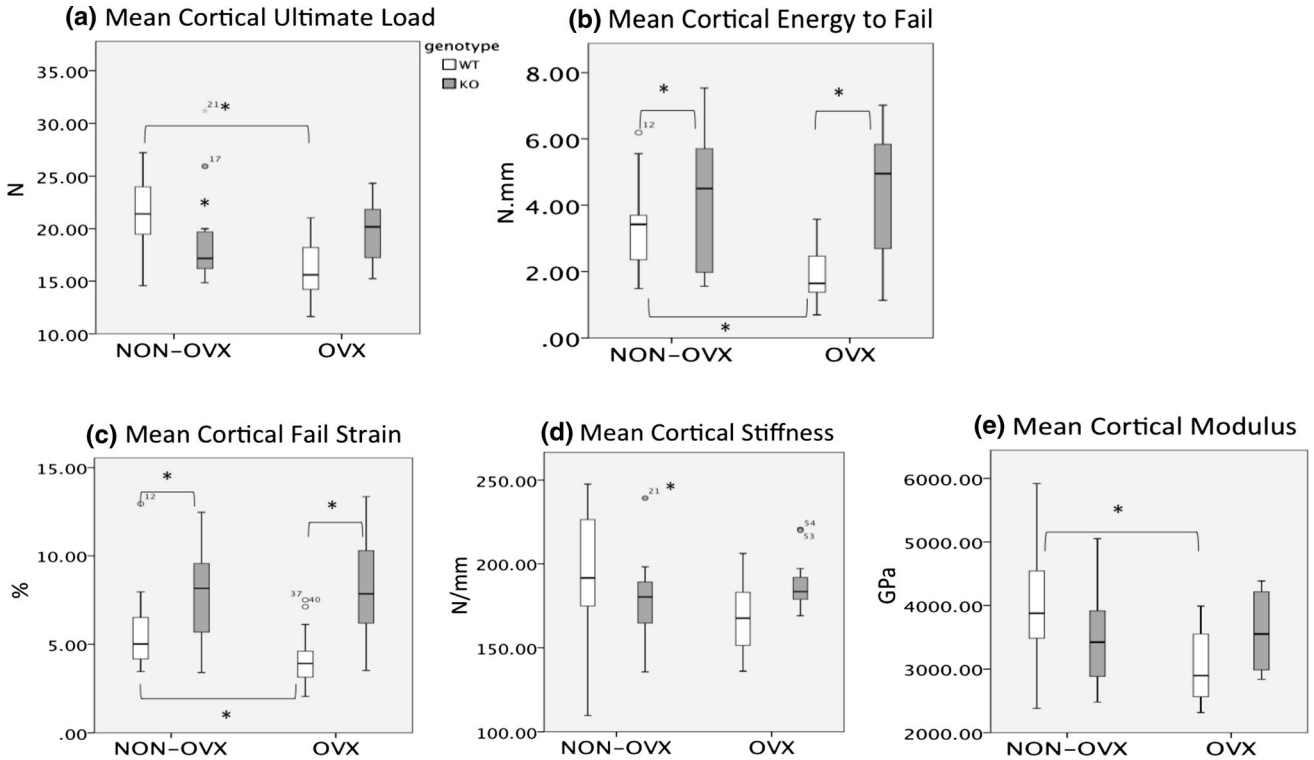

Fig. 4 FLNA-KO femora are protected from estrogen-mediated post-menopausal changes in bone mechanical properties. FLNA-KO/KO-OVX femora are more ductile than WT/WT-OVX bones. Ultimate load reveals a significant effect due to OVX in the WT group (Fig. 4**a**). Structurally, FLNA-KO femora require more energy to fracture and have a higher fail strain compared to WT femora (Fig. 4**b**, **c**, respectively). There is a significant effect due to OVX in the WT groups for both the structural and material properties of femora, which, in turn, are significantly different than the KO groups. Stiffness as well as Young's modulus is significantly decreased in the WT-OVX group (Fig. 4**d**, **e**). FLNA-KO groups remain unchanged from one another. *Stars* represent data that are significantly decreased ($p < 0.05$)

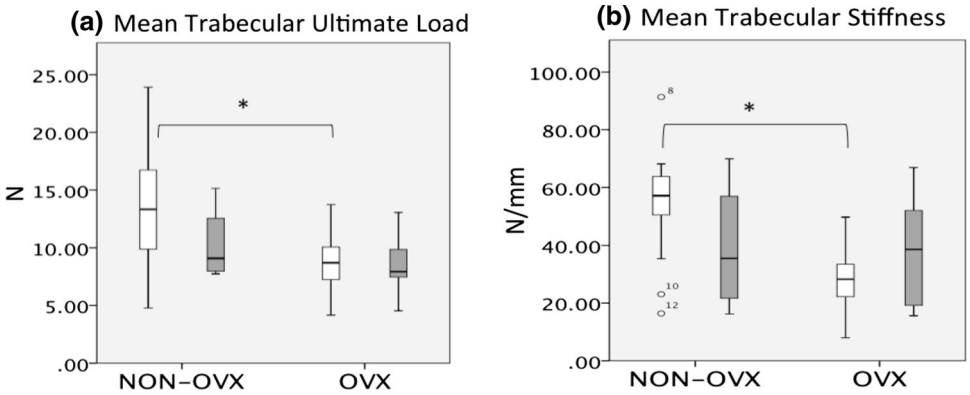

Fig. 5 FLNA-KO vertebrae are protected from estrogen-mediated post-menopausal changes in bone mechanical properties. Vertebral compression data show expected decreases in the WT-OVX group for ultimate load and stiffness. FLNA-KO groups remain unchanged from one another (Fig. 5**a**, **b**). *Stars* represent data that are significantly decreased ($p < 0.05$)

and FLNA-KO-OVX 11-month groups. Since there is a 6-month gap between the 5- and 11-month groups, we postulated that we were unable to observe changes due to OVX in the 11-month group. Therefore, a 6-month group was introduced in which mice were sacrificed 5 weeks post-OVX. The 6-month group revealed an expected significant increase in number of osteoclasts and number of osteoclasts per bone surface in WT-OVX vertebrae compared to WT vertebrae. No significant differences were reported among FLNA-KO and FLNA-KO-OVX groups (Table 4).

Table 4 TRAP histomorphometry of 6-month non-OVX versus OVX vertebrae

Parameters	WT	WT-OVX	KO	KO-OVX	*p* value WT	*p* value KO
Oc.S	1.13 ± 0.57	1.89 ± 0.47	0.62 ± 0.39	0.97 ± 0.12	0.02*	0.06
Oc.S/BS	0.12 ± 0.085	0.16 ± 0.036	0.08 ± 0.047	0.1 ± 0.05	0.16	0.38
N.Oc	37.67 ± 11.11	56.22 ± 15.06	26.58 ± 15.83	29.37 ± 9.17	0.02*	0.72
N.Oc/BS	3.75 ± 2.13	8.33 ± 2.92	3.35 ± 1.78	4.57 ± 2.57	0.006*	0.3

There was a significant increase in osteoclast surface number of osteoclasts and number of osteoclasts per bone surface in the 6-month WT-OVX group. No significant differences were reported among 6-month FLNA-KO groups. Table represents mean ± SD

* Significant difference at $p < 0.05$

Table 5 Static histomorphometry of 6-month non-OVX versus OVX vertebrae

Parameters	WT	WT-OVX	KO	KO-OVX	*p* value WT	*p* value KO
OS/BV	0.13 ± 0.011	0.02 ± 0.058	0.02 ± 0.02	0.03 ± 0.028	0.0001*	0.24
OS	0.73 ± 0.289	0.42 ± 0.39	0.41 ± 0.27	0.33 ± 0.199	0.09	0.44
OS/BS	0.17 ± 0.05	0.07 ± 0.025	0.08 ± 0.039	0.09 ± 0.062	0.0001*	0.55
O.Wi	7.03 ± 1.5	4.93 ± 1.81	4.76 ± 2.43	6.35 ± 1.99	0.02*	0.13

Static histomorphometry revealed significant decreases in osteoid volume/bone volume, osteoid surface/bone surface and osteoid width in the 6-month WT-OVX group. Significant differences were not observed among 6-month KO groups. Tables represent mean ± SD

* Significant difference at $p < 0.05$

Table 6 Dynamic histomorphometry of 6-month non-OVX versus OVX vertebrae

Parameters	WT	WT-OVX	KO	KO-OVX	*p* value WT	*p* value KO
MS/BS	0.33 ± 0.093	0.28 ± 0.048	0.27 ± 0.091	0.28 ± 0.066	0.25	0.69
Interlab.Wi	19.12 ± 6.84	10.3 ± 4.29	12.86 ± 7.94	10.33 ± 7.24	0.02*	0.5
MAR	2.73 ± 0.98	1.47 ± 0.61	1.84 ± 1.13	1.48 ± 1.03	0.02*	0.5

The single and double calcein-green labels for dynamic histomorphometry on un-decalcified histological sections revealed significant decreases in the following parameters: mineralizing surface/bone surface, inter-label distance, and mineral apposition rate in 6-month WT-OVX vertebrae. Significant differences were not observed among 6-month KO groups. All results are reported as means in tables and mean ± SD in graphs. Table represents mean ± SD

* Significant difference at $p < 0.05$

In the 6-month group, static histomorphometry revealed significant decreases in osteoid volume per bone volume, osteoid surface per bone surface and osteoid width in 6-month-old WT-OVX vertebrae compared to WT vertebrae (Table 5). Significant differences were not observed between FLNA-KO and FLNA-KO-OVX vertebrae. The single and double calcein-green labels for dynamic histomorphometry on un-decalcified histological sections revealed significant decreases in the following parameters: mineral apposition rate, inter-label distance, bone formation rate per bone surface, and bone formation rate per bone volume in WT-OVX trabeculae compared to WT trabeculae. Significant differences were not observed between FLNA-KO and FLNA-KO-OVX trabeculae (Table 6).

Discussion

The results of this study suggest that FLNA-KO bones show a mild osteoporotic phenotype compared to WT bones. Skeletal aging-related osteoporosis was not altered by the deletion of FLNA. However, FLNA-KO bones were protected from estrogen-mediated post-menopausal changes in bone properties. Due to the long duration of time between the 5- and 11-month groups, OVX-related differences in osteoclast and osteoblast behavior were not visible histologically in the 11-month-old OVX group. Since osteoclast and osteoblast activities must be observed 4–6 weeks post-OVX, the 6-month group was introduced to observe changes in bone due to OVX at the tissue level. When OVX is introduced, FLNA-KO bones appear to be

protected from estrogen-mediated post-menopausal osteoporosis. Our observations suggest that estrogen depletion has no significant effect on bone turnover rates in bones lacking FLNA. Under normal circumstances, estrogen depletion results in high turnover rates leading to decreases in bone mineral density, bone microarchitecture, and mechanical properties. These parameters remain intact in FLNA-KO due to low bone resorption and formation rates.

The decrease in bone turnover rate in FLNA-KO bones may be explained by insufficient OCG leading to smaller osteoclasts with fewer nuclei. Previous literature on FLNA in vitro reported deficiencies in OCG in FLNA-null monocytes. Under normal in vitro plating densities, FLNA-null osteoclasts were smaller, less numerous, and contained less nuclei per osteoclast. Quantification of osteoclasts in vivo in the distal femoral head revealed similar results, illustrating the in vivo physiological relevance of FLNA in OCG [20]. These findings in conjunction with the findings in this study suggest that FLNA-null osteoclasts are smaller and fewer in vivo, which may influence their resorptive capacity. Consequently, in vivo and in vitro situations do not always complement each other. Based on previous in vitro findings done by Leung et al. [20], the 5-month FLNA group should have displayed an osteopetrotic phenotype resulting in stronger bones with higher bone mineral density. On the contrary, 5-month FLNA bones were osteopenic displaying weaker bones lower bone mineral density. The FLNA osteoporosis group, on the other hand, correlated positively with Leung et al. [20] in vitro findings.

Existing literature reports that osteoclast size and number are correlated with osteoclast function [24, 25]. Lees and Heersche show that an increase in the number of larger osteoclasts was paralleled with an increase in the size and depth of their resorption pits. Additionally, when resorption was expressed as the amount of bone resorbed per osteoclast nucleus, larger osteoclasts resorbed more per nucleus, suggesting that large osteoclasts, as a population, are more effective at resorbing bone than small osteoclasts. Interestingly, when osteoclasts were plated at one-fifth the standard density, the amount of bone resorbed per osteoclast decreased considerably, indicating that resorptive activity is also affected by cell density of osteoclasts and/or of other cells present [20, 25]. Our findings suggest that the smaller FLNA-KO osteoclasts have a reduced capacity for bone resorption in vivo. This explains why the down-regulation of estrogen has no negative impact on bone microarchitecture in mice lacking FLNA.

FLNA-KO cortices displayed significant increases in energy to fail and toughness, indicating that they are tougher and more ductile than WT femora. The increased toughness and ductility indicate that FLNA-KO cortices may have significant alterations in the biochemical and structural composition of the mineral and organic components of the bone matrix compared to WT cortices. This phenomenon was not evident in FLNA-KO trabeculae, however. Takahata et al. observed that the mechanisms of plastic deformation (ductility) in bone are different between bending (cortical) and compressive (trabecular) loading. Under tensile and shear stresses, as the bone yields and failure initiates in the form of micro-cracks through the mineral phase, the collagen matrix can act as a significant toughening mechanism against failure [26]. Additionally, since trabecular remodeling is much quicker compared to cortical remodeling, it is possible that this phenomenon is slightly masked in the vertebrae of FLNA-KO bones.

In terms of the organic components of the bone matrix, collagen maturity in bone is negatively correlated with bone formation rates; an increase in collagen maturity reflects lower rates of bone formation. The mature collagen matrix contains more pyridinoline cross-links, which may be associated with the ductility of bone that was observed in this study. Collagen cross-linking is an important determinant of bone strength, especially in post-yield mechanical properties [26–30]. The decrease in bone turnover rate in FLNA-KO bones due to insufficient OCG producing mature osteoclasts may lead to the presence of more "mature" collagen in the FLNA-KO bones resulting in larger plastic zones and tougher bones.

Another explanation for the lack of effect of OVX in FLNA-KO bones may be that FLNA and estrogen regulate the same pathways. Specifically, estrogen and FLNA are both involved in regulating IL-1 mediated TNF-induced OCG [31–34]. IL-1 is a cytokine that mediates the osteoclastogenic effect of TNF by enhancing stromal cell expression of RANKL and directly stimulating differentiation of osteoclast precursors [31, 33]. RANKL is a TNF family member that is expressed on the surface of osteoblasts and is essential for osteoclast differentiation. Binding of RANKL to its receptor, RANK, activates a cascade of transcription factors that are known to be important for OCG. RANK, similar to other TNF receptor family members, interacts with TNF receptor-associated factors (TRAFs), which, in turn, act as adaptors to downstream signaling pathways. Of the six known TRAFs, RANK interacts with TRAFs 1, 2, 3, and 5 in a membrane-distal region of the cytoplasmic tail, and with TRAF6 at a distinct membrane-proximal binding motif. TRAF6 appears to be the most crucial adapter for RANK signaling during OCG in vivo and in vitro, indicating that RANKL-induced signaling is predominantly mediated by TRAF6 during OCG. Additionally, TRAF6 seems to be the primary TRAF protein utilized in IL-1 signaling. Literature reveals that FLNA inhibits NF-κB activation induced via TNF, interleukin-1, and TRAF6. Additionally, TNF fails to activate NF-κB in a human melanoma cell line deficient in FLNA. Reintroduction of FLNA into these cells restores the TNF response [31–33].

In the wild-type situation, estrogen suppresses cytokines including IL-1, IL-6, TNF, GM-CSF, M-CSF, PGE2, and RANKL [32, 33]. In addition, estrogen prolongs osteoblast lifespan and increases production of TGF-B [33, 34]. Conversely, estrogen depletion results in an increase in the aforementioned cytokines, prolonged osteoclast lifespan, and an increase in osteoblast apoptosis. Although increased bone resorption induced by OVX may be explained by the cumulative effects of these cytokines, IL-1 and TNF specifically play a prominent causal role in bone loss associated with estrogen deficiency. A study done by Kimble et al. revealed that OVX increased the mononuclear cell secretion of IL-1, TNF, and the stromal cell production of M-CSF. OCG was decreased by in vivo treatment of donor mice with either estrogen or a combination of the IL-1 inhibitor, IL-1 receptor antagonist, and the TNF inhibitor [35–37].

The study done by Kimble et al. indicates that estrogen-depleted FLNA-KO mice have down-regulated TNF and IL-1 expression via the absence of FLNA and a simultaneous up-regulation of these cytokines via the absence of estrogen. We speculate that this would result in a canceling out effect whereby estrogen deficiency does not result in post-menopausal loss of bone architecture and quality in mice lacking FLNA.

Since there are three Filamin isoforms, it is speculated that Filamin B or C may be compensating for the loss of Filamin A. This may explain the observed mild phenotype between WT and FLNA-KO bones and between aging groups. Further research will need to explore these findings. Conclusively, FLNA-null bones appear to be weaker at 5 months of age compared to their WT counterparts. Skeletal aging, however, does not appear to differ between WT and FLNA-KO bones. Our most intriguing finding is that FLNA-KO bones are protected from estrogen-mediated post-menopausal osteoporosis as well as being more ductile than their WT counterparts.

Acknowledgments The work was supported by a CIHR operating grant to Dr. Michael Glogauer. Stephanie Goldberg participated in making substantial contributions to conception and design, acquisition of data and analysis, and interpretation of data. Stephanie Goldberg, Marc Grynpas, and Michael Glogauer participated in drafting the manuscript and revising it critically for important intellectual content. Marc Grynpas and Michael Glogauer approved the final version of the submitted manuscript, and all three authors agreed to be accountable for all aspects of the work in ensuring that questions related to the accuracy or integrity of any part of the work were appropriately investigated and resolved. Judah Glogauer participated in data acquisition.

Conflict of interest Stephanie Goldberg, Judah Glogauer, Marc Grynpas, and Michael Glogauer have no conflicts of interest to disclose.

Human and Animal Rights and Informed Consent All procedures followed were in accordance with the ethical standards of the responsible committee on human experimentation (institutional and national) and with the Helsinki Declaration of 1975, as revised in 2000 (5). Informed consent was obtained from all patients for being included in the study.

References

1. Shipman P, Walker A, Bichell B (1985) The human skeleton. USA Harvard University Press, Massachusetts
2. Rucci N (2008) Molecular biology of bone remodeling. Clin Cases Miner Bone Metab 5(1):49–56
3. Boyle WJ, Simonet WS, Lacey DL (2003) Osteoclast differentiation and activation. Nature 423:337–342
4. Saltel F, Destaing O, Bard F, Eichert D, Jurdic P (2004) Apatite-mediated actin dynamics in resorbing osteoclasts. Mol Biol Cell 15:5231–5241
5. Manolagas SC (2000) Birth and death of bone cells: basic regulatory mechanisms and implications for the pathogenesis and treatment of osteoporosis. Endocr Rev 21:115–137
6. Cooper C (1999) Epidemiology of osteoporosis. Osteoporos Int 9:S2–S8
7. Glaser DL, Kaplan FS (1997) Osteoporosis. Definition and clinical presentation. Spine 22:12S–16S
8. Kanis J (2002) Diagnosis of osteoporosis and fracture risk. Lancet 359:1929–1936
9. Garnero P, Sornay-Rendu E, Chapuy MC et al (1996) Increased bone turnover in late postmenopausal women is a major determinant of osteoporosis. J Bone Miner Res 11:337–349
10. Pacifici R (1996) Estrogen, cytokines, and pathogenesis of postmenopausal osteoporosis. J Bone Miner Res 8:1043–1051
11. Riggs BL, Khosla S, Melton L (1998) A unitary model for involutional osteoporosis: estrogen deficiency causes both type I and type II osteoporosis in postmenopausal women and contributes to bone loss in aging men. J Bone Miner Res 13:763–773
12. Jaffe AB, Hall A (2005) Rho GTPases: biochemistry and biology. Annu Rev Cell Dev Biol 21:247–269
13. Wang Y, Lebowitz D, Sun C, Thang H, Grynpas MD, Glogauer M (2008) Identifying the relative contributions of Rac1 and Rac2 to osteoclastogenesis. J Bone Miner Res 23:260–270
14. Ory S, Brazier H, Pawlak G, Blangy A (2005) Rho GTPases in osteoclasts: orchestrators of podosome arrangement. Eur J Cell Biol 87:469–477
15. Stossel TP, Condeelis J, Cooley L et al (2001) Filamins as integrators of cell mechanics and signalling. Nat Rev Mol Cell Biol 2:138–145
16. Popowicz GM, Schleicher M, Noegel AA, Holak TA (2006) Filamins: promiscuous organizers of the cytoskeleton. Trends Biochem Sci 31:411–419
17. Flanagan LA, Chou J, Falet H, Neujahr R, Hartwig JH, Stossel TP (2001) Filamin A, the Arp2/3 complex, and the morphology and function of cortical actin filaments in human melanoma cells. J Cell Biol 155:511–517
18. Steenblock C, Heckel T, Czupalla C, Santo A, Niehage C, Sztacho M, Hoflack B (2014) The Cdc42 guanine nucleotide exchange factor FGD6 coordinates cell polarity and endosomal membrane recycling in osteoclasts. J Biol Chem 289(26): 18347–18359
19. Sheen VL, Dixon PH, Fox JW et al (2001) Mutations in the X-linked filamin 1 gene cause periventricular nodular heterotopia in males as well as in females. Hum Mol Genet 10:1775–1783
20. Leung R, Wang Y, Cuddy K, Sun C, Magalhaes J, Grynpas MD, Glogauer M (2010) Filamin A regulates monocyte migration through Rho small GTPases during osteoclastogenesis. J Bone Miner Res 25:1077–1091

21. Feng Y, Chen MH, Moskowitz IP et al (2006) Filamin A (FLNA) is required for cell-cell contact in vascular development and cardiac morphogenesis. Proc Natl Acad Sci USA 3:19836–19841
22. Clausen BE, Burkhardt C, Reith W, Renkawitz R, Forster I (1999) Conditional gene targeting in macrophages and granulocytes using LysMcre mice. Transgenic Res 8:265–277
23. Parfitt AM, Drezner MK, Glorieux FH et al (1987) Bone histomorphometry: standardization of nomenclature, symbols, and units. Report of the ASBMR179 Histomorphometry Nomenclature Committee. J Bone Miner Res 2:595–610
24. Goldberg S, Georgiou J, Glogauer M, Grynpas MD (2012) A 3D scanning confocal imaging method measures pit volume and captures the role of Rac in osteoclast function. Bone 51:145–152
25. Lees RL, Heersche JN (1999) Macrophage colony stimulating factor increases bone resorption in dispersed osteoclast cultures by increasing osteoclast size. J Bone Miner Res 6:937–945
26. Takahata M, Maher JR, Juneja SC, Inzana J, Xing L, Schwarz EM, Berger AJ, Awad HJ (2012) Mechanisms of bone fragility in a glucocorticoid-treated mouse model of rheumatoid arthritis—implications for insufficiency fracture risk. Arthritis Rheum 11:3649–3659
27. Viguet-Carrin S, Garnero P, Delmas PD (2006) The role of collagen in bone strength. Osteoporos Int 17:319–336
28. Von der Mark K (1999) Components of the organic extracellular matrix of bone and cartilage: structure and biosynthesis of collagens. In: Seibel M, Robins S, Bilezikian J (eds) Dynamics of bone and cartilage metabolism. Elsevier Inc, Amsterdam, pp 3–18
29. Hansson T, Roos B, Nachemson A (1980) The bone mineral content and ultimate compressive strength of lumbar vertebrae. Spine 5:46–55
30. Leichter I, Margulies JY, Weinreb A et al (1982) The relationship between bone density, mineral content, and mechanical strength in the femoral neck. Clin Orthop Relat Res 163:272–281
31. Hayashi K, Altman A (2006) Filamin A is required for T cell activation mediated by protein kinase C-theta. J Immunol 177(3):1721–1728
32. Sasaki A, Masuda Y, Ohta Y, Ikeda K, Watanabe K (2001) Filamin associates with Smads and regulates transforming growth factor-beta signaling. J Biol Chem. 21:17871–17877
33. Pacifici R, Rifas L, McCracken R, Avioli LV (1990) The role of interleukin-1 in postmenopausal bone loss. Exp Gerontol 25:309–316
34. Hahnel R, Gschwendt M (1995) The interaction between protein-kinase-C (PKC) and estrogens. Int J Oncol 10:11–16
35. Marino M, Galluzzo P, Ascenzi P (1996) Estrogen signaling multiple pathways to impact gene transcription. Curr Genomics 8:497–508
36. Kimble RB, Srivastava S, Ross FP, Matayoshi A, Pacifici R (1996) Estrogen deficiency increases the ability of stromal cells to support murine osteoclastogenesis via an interleukin-1 and tumor necrosis factor-mediated stimulation of macrophage colony-stimulating factor production. J Biol Chem 46:28890–28897
37. Leonardi A, Ellinger-Ziegelbauer H, Franzoso G, Brown K, Siebenlist U (2000) Physical and functional interaction of Filamin (actin-binding protein-280) and tumor necrosis factor receptor-associated factor 2. J Biol Chem 275:271–278